Estimates of Spatial Degrees of Freedom

KLAUS FRAEDRICH, CHRISTINE ZIEHMANN, AND FRANK SIELMANN

Meteorologisches Institut, Universität Hamburg, Hamburg, Germany

(Manuscript received 23 January 1994, in final form 27 June 1994)

ABSTRACT

The spatial degrees of freedom (dof) of atmospheric flows are estimated by comparing the variance of the theoretical standardized chi-squared distribution with the sum of the squared eigenvalues of a spatial correlation matrix, dof = $N^2/\sum_{i=1}^{N}\lambda_i^2$. The dof statistics are applied to monthly anomalies of ten-year datasets using daily 1000-mb heights of the T-21 representation of observations (ECMWF analyses 1980–89) and model simulations (ECHAM2) for the Northern Hemisphere mid- and higher latitudes (NH) and the eastern North Atlantic/European sector. Scales are distinguished by using unfiltered, low-, and bandpass filtered datasets. The following results are of interest: (i) The dofs of the observations are in qualitative agreement with the number of distinct weather types defined by phenomenological studies of the synoptic climatology on the hemispheric and regional scale. (ii) The larger number of dofs in summer (than in winter) can be associated with the reduced forecast performance of NWP models in the anomaly correlation sense. (iii) The larger number of ECHAM2 dofs for bandpass filtered anomalies (compared with observations) reveals the model's inability to activate as few modes as the atmosphere. (iv) Interannual variability is characterized by dof differences between daily anomalies taken from individual monthly averages and from the climate mean.

1. Introduction

Large-scale circulation patterns of recurrent weather episodes are a fundamental property of atmospheric dynamics. These processes are being studied since spatial and temporal data coverage was assumed to be sufficient. First analyses of the large-scale weather were phenomenological classifications of synoptic processes. They lead to large-scale circulation patterns of the Northern Hemisphere (NH) extratropics (Dzerdzeevskii 1975), to the Grosswetterlagen of the eastern North Atlantic/European sector (Hess and Brezowski 1977; Gerstengarbe and Werner 1993), and to the British Isles weather types (Lamb 1972). The associated numbers of different weather patterns or modes reveal hierarchies: The largest scale (NH extratropics poleward of 30°N, Dzerdzeevskii 1975) is classified by 42 circulation types (including an indeterminable one), which are effectively reduced to 36 in individual summer or winter seasons. These types can be combined to form 13 elementary circulation patterns that, in turn, can be categorized into four principal groups (zonal mean, zonally asymmetric, meridional, and mixed). In the eastern North Atlantic/European sector there are 29 (plus one indeterminable) weather patterns defined by the Grosswetterlagen catalog (Hess and Brezowski 1977); they are embedded in ten major regimes, which again can be combined into three basic large-scale circulation forms (zonal, meridional, and mixed). On a smaller scale (50°–60°N; 10°W–2°E) the British Isles weather (Lamb 1972) is classified in terms of seven types. Other regional classification schemes are also known (Barry and Perry 1973).

These circulation types are identified by subjective "pattern recognition" of the centers of action, the steering of cyclones and anticyclones, weather regimes, etc., that characterize the sea level pressure fields on a day-to-day basis. More objective methods to identify weather regimes have been used recently. They are based on the statistical analysis of a phase space spanned by a few spatial empirical orthogonal functions (EOFs) deduced from time series of weather maps. Centroids derived from a subsequent cluster analysis in phase space are identified as weather regimes (e.g., Molteni et al. 1990; Vautard 1990; Cheng and Wallace 1993; Kimoto and Ghil 1993a,b).

The numbers of independent circulation modes may also be interpreted in terms of the degrees of freedom (dof) of flow fields embedded in the geometric space. In this sense they define the dimensionality of the atmospheric circulation. These dofs are traditionally estimated by two different methods: (i) The squared distances between independent daily weather maps (Lorenz 1969, dof ~ 44) and between daily weather maps and the climate mean (Toth 1994, dof ~ 24) form chi-squared distributions, if the weather maps are Gaussian distributed. Their degrees of freedom are de-

Corresponding author address: Dr. Klaus Fraedrich, Meteorologisches Institut, Universität Hamburg, Bundesstrasse 55, Hamburg D-20146 Germany.
E-mail: fraedrich@dkrz.d400.de

termined by fitting the observed to theoretical probability densities. (ii) Pattern correlation coefficients between weather maps lead to a normally distributed population (after being subjected to the Fisher z-transform) whose standard deviation depends on the number of statistically independent grid points. Filtered and unfiltered datasets have been analyzed (Horel 1985, unfiltered daily 500-mb height: dof $\sim$ 30–37; small wavenumbers $k < 4$: dof $\sim$ 21–27), and low-frequency regimes (Wallace et al. 1991: dof $\sim$ 20; and Toth 1994: dof $\sim$ 14). Finally, significance tests (Livezey and Chen 1983: dof $\sim$ 35) can be used as another method. The technique introduced here is related to method (i) analyzing squared distances from the climate mean. While Lorenz (1969) and Toth (1994) fit distributions, we explicitly make use of a relationship between the degrees of freedom and the variance of the chi-squared distribution.

The purpose of this paper is to present estimates of the statistical dimension (degrees of freedom or dof) of atmospheric fields, simplifying the method of fitting chi-squared distributions. As spatial (weather) patterns may be described in terms of empirical orthogonal eigenvectors, the method of estimating dofs is reduced to estimates of (the sum of squared) eigenvalues of the spatial correlation matrix (section 2). The degrees of freedom are introduced as a scalar measure of the general circulation, which provides some useful insight into the underlying dynamics (section 3) both for observational and for model simulation diagnostics. Discussion follows in section 4, suggesting dofs as scalar measures for atmospheric diagnostics.

2. Analysis of the degrees of freedom

The degrees of freedom (dof) of a system, whose states are normally distributed and described by a vector time series, $X_i(t)$, of N components, can be deduced from the distribution of the squared sum, V^2, of the normalized state variables, $X, Y, Z, \ldots$ (deviations from the ensemble mean normalized by their respective standard deviation). This can be illustrated in a simple way by a set of two ($N = 2$), $[X(t), Y(t)]$, variables in terms of normalized anomalies:

$$V^2(N = 2) = (X)^2 + (Y)^2. \tag{2.1}$$

Now, if X and Y are Gaussian (standard normalized) and independent, the sum V^2 is chi-squared distributed with two degrees of freedom. If they are not independent, dof < 2. If this chi-squared variable, $V^2(N = 2)$, is standardized by dividing it by the number of variables, $N = 2$, then its probability density function (pdf) (i.e., the standardized sum of the squares) should follow the chi-squared pdf standardized by its degrees of freedom:

$$\text{pdf}\left\{\frac{V^2(N=2)}{N}\right\} = \text{pdf}\left\{\frac{X^2 + Y^2}{2}\right\} = \text{pdf}\left\{\frac{\chi^2_{\text{dof}}}{\text{dof}}\right\}. \tag{2.2}$$

The normalized distribution, pdf(V^2), composed of observed variables $X_i(t)$, can be fitted to the chi-squared distribution to obtain an estimate of the associated degrees of freedom. Lorenz (1969) analyzed the distribution of distances between weather maps; Toth (1994) analyzed the distances from the climate mean. Both kinds of distance measures are assumed to be Gaussian distributed. The fitting can be further simplified realizing X and Y as Gaussian-distributed variables with zero mean. Then it is sufficient to compare only the variances (var) of the empirical standardized $V^2/2$ distribution with the variance of the standardized chi-squared distribution, $\chi^2_{\text{dof}}/\text{dof}$. With the variance operator var and realizing that $N = 2$, one obtains

$$\text{var}\left\{\frac{X^2}{2} + \frac{Y^2}{2}\right\} = \text{var}\left\{\frac{\chi^2_{\text{dof}}}{\text{dof}}\right\} = \frac{2}{\text{dof}} \tag{2.3}$$

because the variance of a chi-squared distribution with dof degrees of freedom is 2 dof. This may be cast in an even more elegant form. The variance var$\{X^2/2 + Y^2/2\}$ of the distribution (2.2) is associated with the covariance of the vector time series (X, Y) with its transpose $(X, Y)^T$. This gives the correlation matrix

$$C = \langle (X, Y)(X, Y)^T \rangle = \begin{pmatrix} 1 & c \\ c & 1 \end{pmatrix},$$

where c is the covariance between X and Y. The eigenvalues and the normalized eigenvectors are $\lambda_1 = 1 + c$, $\epsilon_1 = \{1/(2)^{1/2}, 1/(2)^{1/2}\}$ and $\lambda_2 = 1 - c$, and $\epsilon_2 = \{1/(2)^{1/2}, -1/(2)^{1/2}\}$. Now we can express the dependent variables X and Y in terms of a linear combination of the two new independent normalized amplitudes η and ξ (or projections onto the eigenvectors ϵ_1 and ϵ_2):

$$X = \frac{(1 + c)^{1/2}}{(2)^{1/2}}\eta + \frac{(1 - c)^{1/2}}{(2)^{1/2}}\xi;$$

$$Y = \frac{(1 + c)^{1/2}}{(2)^{1/2}}\eta - \frac{(1 - c)^{1/2}}{(2)^{1/2}}\xi.$$

Thus, the variance of the squared sum, $V^2 = X^2 + Y^2 = (1 + c)\eta^2 + (1 - c)\xi^2$, yields

$$\text{var}\{X^2 + Y^2\} = \lambda_1^2 \text{var}\{\eta^2\} + \lambda_2^2 \text{var}\{\xi^2\} = (1 + c)^2 \text{var}\{\eta^2\} + (1 - c)^2 \text{var}\{\xi^2\} = 4(1 + c^2).$$

Both squared amplitudes, η^2 and ξ^2, are individually chi-squared distributed with one degree of freedom (dof = 1), so that var$\{\eta^2\}$ = var$\{\xi^2\} = 2$ or 2 dof, because

the variance of a chi-squared variable with dof = 1 is 2. Substitution into (2.3) finally yields the relation between the degrees of freedom, the eigenvalues, and the correlation coefficient:

$$\text{dof} = \frac{N^2}{\lambda_1^2 + \lambda_2^2} = \frac{2}{1 + c^2}, \tag{2.4}$$

where c^2 is the fraction of the total variance of X explained by Y and $N = 2$. Note that the sum of the eigenvalues represents the overall variance of the system in terms of the linearly independent contributions of each of the individual N eigenvectors; the variance of the associated squared amplitudes of these eigenvectors is twice their squared variance fractions.

The generalization to more than two state variables, N, is given by (appendix A)

$$\text{dof} = N^2 \Big/ \sum_{i=1}^{N} \lambda_i^2. \tag{2.5}$$

The application of this method requires only the derivation of the correlation matrix C and all of its eigenvalues. Then, Eq. (2.5) gives the associated statistical estimate of the degrees of freedom (or statistical dimension) of a dynamical system. Note that the vector variable, $X_i(t)$ with $i = 1, \cdots, N$, consists of N components; they are normalized by subtracting the ensemble mean $\langle X_i \rangle$ and dividing by the standard deviation, s_x.

It should be noted that the variables η and ξ are independent only under the assumption of multinormality of the data. Therefore the covariance between η^2 and ξ^2 vanishes. In general the above procedure of projection on eigenvectors of the correlation matrix leads to only uncorrelated η and ξ, and the covariance between η^2 and ξ^2 is not necessarily zero but, in general, small compared to $\text{var}(\eta^2)$ and $\text{var}(\xi^2)$.

An example for non-Gaussian variables shows that overestimating the spatial dimension by this method is possible. This can be directly inferred from analyzing a circle embedded in the two-dimensional (x, y) space: $x = \sin(t)$, $y = \cos(t)$ with parameter t (embedding dimension two). The related correlation matrix is the identity matrix with eigenvalues $\lambda_1, \lambda_2 = 1$ so that the dimension yields (2.5) dof = 2; but a circle has the topological dimension one.

We note in passing that the dofs discussed here characterize linearly independent spatial properties in an essentially multinormally distributed phase space, whereas nonlinear relations are analyzed by means of similarity measures; they do not follow the linear superposition principle. Therefore, it is not surprising to obtain the overestimate in the case of the circle. In this sense the spatial dofs are possibly closer to an estimate of the embedding dimension than of the topological dimension of the object. Finally, this method of estimating dofs by the (sum of squared eigenvalues) appears to provide some additional insight into fitting the chi-squared distribution.

The confidence limits of the dof-estimates may be deduced from the confidence in the eigenvalues λ_i following a rule of thumb (North et al. 1982): $\delta\lambda_i = \pm 2\lambda_i (2/M)^{1/2}$, which depends on the number of realizations M (independent weather maps). Substituting this into (2.5) gives the confidence interval $\text{dof}_- < \text{dof} < \text{dof}_+$ with

$$\text{dof}_\pm = \{1 \mp 2(2/M)^{1/2}\}^{-2}\text{dof}.$$

Thus, the upper and lower limits can be described in percent of the estimated dofs for given sample size M. The data analyzed in the following are daily geopotential heights from a 10-year period. Thus, for a calendar month there is a sample size of 300, which consists of about $M = 100$ independent realizations corresponding to a 3-day decorrelation time. For monthly estimates this leads to lower and upper confidence limits of about −40% and +90%. These confidence limits show that 10 years is a small sample for this kind of statistical estimate, because some of the features of the seasonal cycle discussed later in the paper fall within these confidence limits.

A final comment of the effect of additive white noise on the dof estimate is in order: Adding white noise to the Lorenz system tends to increase the dofs, but it does not seriously affect the result, as long as the noise level remains small compared with the "natural" variance of the variables.

3. Midlatitude height fields

The *data* analyzed are daily geopotential height fields from a 10-year period. The spatial resolution is defined by the T-21 spectral representation of observed ECMWF analyses and ECHAM2 (European Center—Hamburg climate model) model data. The observations are taken from daily ECMWF analyses 1980–89 (available in T-63 resolution from MPI for Meteorology, Hamburg and Meteorology Department, University of Köln). The model data consist of a 10-year daily dataset (3600 days) taken from the 23-year long control run of the ECHAM2 model with a climatological annual cycle (Roeckner et al. 1992; available from MPI for Meteorology). The T-21 spectral fields are transformed to a Gaussian grid. In the meridional direction the data are weighted by the cosine of latitude. Thus almost equidistant fields are obtained for the subsequent analysis.

Two *spatial domains* are chosen: the Northern Hemisphere (NH) midlatitudes (30.5°–74.7°N) and the eastern North Atlantic/European sector (30.5°–74.7°N; 61.9°W–33.8°E). For comparison, the Southern Hemisphere (SH) midlatitudes (30.5°–74.7°S) are also analyzed. The phenomenological classifications of weather regimes or Grosswetter types cover similar domains: The large-scale circulation pat-

terns of the whole extratropical NH (Dzerdzeevskii 1975) and the eastern North Atlantic/European sector, which is a key area for some regional classifications (e.g., Hess and Brezowski 1977; Lamb 1972). Various *timescales* are chosen to represent both long and short period fluctuations: Unfiltered, low-pass (lp) (10–90 days), and bandpass (bp) (2.5–6 days) filtered time series of daily data are analyzed [using the filters introduced by Blackmon (1976) and Blackmon and Lau (1980)] to distinguish the number of independent modes associated with different scales. All datasets are sampled as follows before being subjected to the dof analysis:

- Anomalies from *monthly means* (lines with open squares in Figs. 1–4): All daily anomalies, $X_i'(t) = X_i - \langle X_i \rangle$, from individual monthly means, $\langle\ \rangle$, (index $i = 1, \cdots 12$) of the same calendar month are combined into one sample of 10 months (1980–89). These dof estimates represent the number of naturally occurring independent weather modes of the respective calendar month. A relatively large number of dofs will be obtained from these combined monthly anomalies because all different types of independent circulation modes are collected in this sample.
- Anomalies from *climate mean* (lines without squares in Figs. 1–4): All daily data of the same calendar months are analyzed in terms of anomalies, $X_i^* = X_i - \langle\langle X_i \rangle\rangle$, deviating from the total average over all 10 calendar months (1980–89), $\langle\langle X_i \rangle\rangle$. This dof estimate allows some insight into the interannual variability and short-term climate fluctuations because they enter through variations about the common mean. The dofs of the anomalies from the climate mean are expected to be smaller than the dofs of anomalies from the monthly means: For large year-to-year variability, the first few eigenvalues of the correlation matrix of the anomalies from the climate mean will be larger than monthly mean anomalies, thus reducing the dofs (2.5).

Two additional points should be noted: Dependence of the dof estimates on the sample size has been analyzed: (i) Enhancing the sample size by joining the monthly datasets to bimonthlys had no influence on the dof estimates; it showed only a smoothing (averaging) of the annual dof curves presented for both the monthly and climate mean anomalies. Reducing the number of points (in time) by one-half also had no influence. This stability of the dof estimates is plausible because the correlation coefficient estimates are relatively stable for sufficiently large sample sizes. (ii) Reducing the number of grid points in space by one-half had almost no influence on the estimates of dimension; a further decrease by one-half; however, led to a dof reduction, because only larger-scale phenomena are being resolved.

Dofs estimated from the (unfiltered, low-, and bandpass filtered) 300- and 500-mb height fields are similar to those of the 1000-mb fields. There is, however, a tendency for dofs to increase with height. The maximum difference between the dofs of the 300- and 1000-mb unfiltered data is only about 4 in August. Therefore, the following analysis will present the annual cycle of dof estimates on a month-to-month basis for 1000-mb heights.

a. Northern Hemisphere midlatitudes

The NH mid- and higher latitudes statistical dimension or dof is deduced (as in section 2) from 1000-mb height fields taken from observational data. The results are presented as described above: the month to month annual cycle of (a) the anomalies from monthly means (line with squares), and (b) the anomalies from climate mean (line without squares). All these dof graphs are computed for the unfiltered, low-, and bandpass filtered weather maps. The results are presented in Fig. 1.

- The *unfiltered* dofs (Fig. 1a) show a marked annual cycle. The dof minimum in February (anomalies from monthly means: 25; anomalies from climate means: 20) increases by about 50% to the peak in July (37; 31). The influence of interannual variability (manifested in the anomalies from climate mean) reduces the dofs by ~5 (which is less than the winter–summer difference of ~10–12). That is, the modes of interannual (climate) variability dominate over the (comparatively less intense) modes occurring in the anomalies from monthly means representing weather processes. Again, it should be noted that some of the differences in the seasonal cycle fall within the confidence limits defined by a 10-year dataset (section 2).
- The *low-pass* filtered data (Fig. 1b) show the expected reduction in the dofs compared to the unfiltered sets. The dofs of the anomalies from monthly means increase by about 50% from a February minimum (~15) to a July maximum (~22). The difference between both anomalies from monthly and climate means is smaller than their difference in unfiltered data.
- The *bandpass* filtered dof (Fig. 1b) values are considerably larger than the unfiltered and low-pass-filtered dofs. The annual cycle is relatively weak and shows a qualitatively different structure for both the anomalies. A level of reduced dofs occurs in September to April (fluctuating about dof ~ 41 and 36, respectively, with minima in November), with more dofs from May to August (varying between dof ~ 45–40).
- For comparison, the *Southern Hemisphere* (SH) dofs are analyzed in the same manner for the 1000-mb height field. The results are presented in Fig. 2. There is almost no indication of an annual cycle, only a small increase of dofs in SH summer. In addition, the bandpass filtered dofs fluctuate about a smaller level (~35) than in the NH (~40). This is also indicated by the low-pass anomaly dofs.

It is worth noting that the hemispheric Grosswetter catalog of Dzerdzeevskii (1975) gives a number of

large-scale circulation types that is comparable to the annually averaged bandpass filtered dofs estimated from the anomalies of the climate mean: the synoptic phenomenology of daily cyclone and anticyclone track patterns is described by about 36 different classes in winter and summer (cf. with 35–45 dofs in the bandpass filtered NH dataset). These classes can be combined to 13 weather regimes, comparable to the 15–17 dofs found in the low-pass-filtered dataset.

More dofs or independent modes occurring in summer than in winter (Fig. 1) coincides with the observation that regimelike behavior appears to be weak in northern summer (Wallace and Zhang 1993). This is also consistent with the conventional wisdom that in the summer local processes (convection, etc.) play a more important role; hence, the relative dominance of large-scale dynamics is diminished.

Finally, anomalies from individual monthly means are analyzed for each year separately. Daily anomalies, $X_i'(t) = X_i - \langle X_i \rangle$, from individual monthly means, $\langle\ \rangle$, (index $i = 1, \cdots 12$) provide a set of 10 monthly degrees of freedom, dof_i, for each calendar month with their respective means ($\langle \mathrm{dof}_i \rangle$; dashed–dotted), standard deviations (vertical bars), and extrema (dotted). The $\langle \mathrm{dof}_i \rangle$ results (Fig. 1a for the unfiltered data) show considerably smaller values (~ 10) and almost no annual cycle compared to the anomalies from monthly and climate means. This statistic characterizes the average number of independent modes within a single month. This low number is not surprising, because each individual month consists of a small number of weather regimes, which differ from year to year. The band- and low-pass filtered anomalies (not shown, $\langle \mathrm{dof}_i \rangle \sim 10$ and 5, respectively) indicate independence after 3 to 6 days.

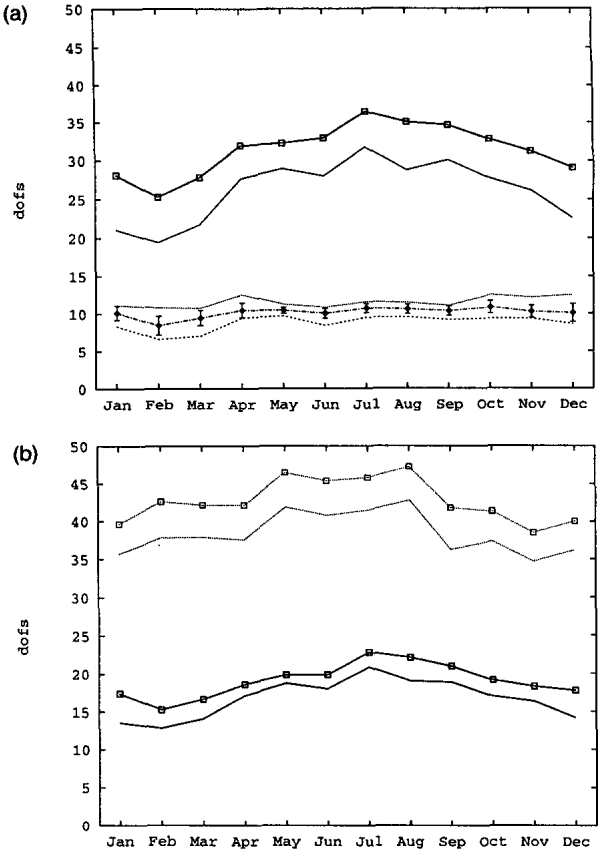

FIG. 1. Annual cycle of the statistical dimension (spatial degrees of freedom or dof) estimated from the T-21 representation of the ECMWF (1980–89) analyses of daily 1000-mb heights of the Northern Hemisphere middle and higher latitudes (30.5°–74.7°N; 180°–180°). (a) Unfiltered anomalies: dof estimates of anomalies from monthly means (with squares); anomalies from climate mean (without squares); and individual monthly anomalies (mean: dashed–dotted; extremes: dashed; standard deviation: vertical bars). (b) Low-pass (full line) and bandpass (dotted line) filtered anomalies.

b. Eastern North Atlantic/European sector

The aim is to analyze a sector in the Northern Hemisphere's middle and higher latitudes whose weather regimes have been phenomenologically investigated (Hess and Brezowski 1977). Furthermore, this sector of the midlatitudes is characterized by the inherent weather variability of the downstream end of the Atlantic storm track, which makes regionalization and downscaling in climate response studies particularly difficult. The results from the dof estimates of the daily 1000-mb heights in the eastern North Atlantic/European sector are shown in Fig. 3.

- The unfiltered dof estimates of both anomalies from monthly and climate means in the eastern North Atlantic/European sector differ by about five in winter and two in summer with annually averaged values of about 13 and 10, respectively (Fig. 3a). Both graphs show a marked annual cycle. There is a winter dof minimum (12 and 7) in February/January with a large dof difference between monthly (12) and climate mean (7) anomalies, and a dof peak (15 and 14) in July. Dof differences between the anomalies from monthly and climate means are largest when interannual variability dominates over the variability of anomalies from monthly means. Thus, the effect of the interannual variability appears to be larger in winter than in summer and is related to low-frequency variability.
- The low-pass filtered eastern North Atlantic/European sector data show the expected reduction in the (dof) number of active modes (Fig. 3b, full line). The increase from February minimum (~ 7) to July maximum (~ 10) remains about 50%. The difference between monthly mean and climate mean dofs is larger in winter than in summer indicating the influence of the year-to-year variability on the low-frequency modes affecting the unfiltered data. The interannual variability from winter to winter appears to be more influential in the Atlantic/European sector than in the NH data.
- The bandpass-filtered dataset (Fig. 3b, dotted line) also reveals a marked annual cycle with smallest values (dof minimum, dof $\sim$ 13–14) in January and the larg-

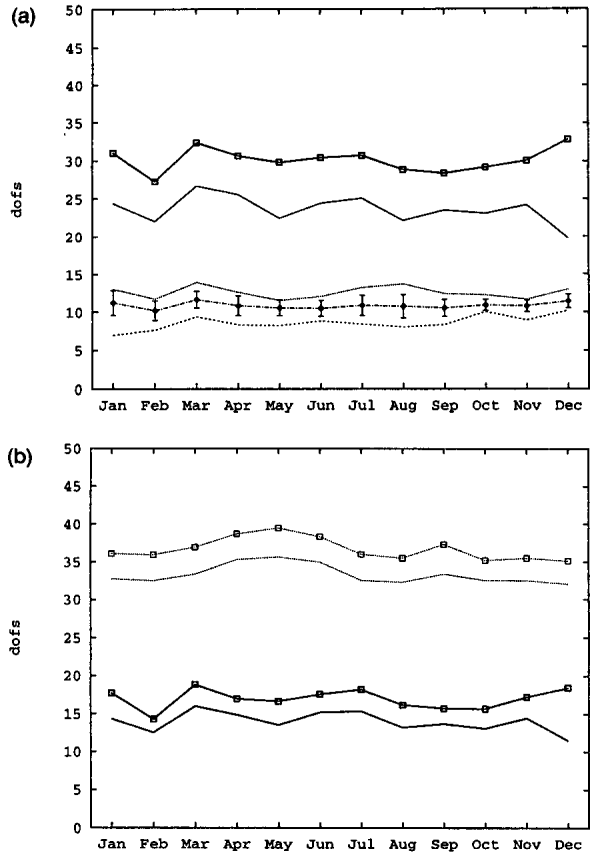

FIG. 2. As in Fig. 1 but for the Southern Hemisphere (30.5°–74.7°N; 180°–180°).

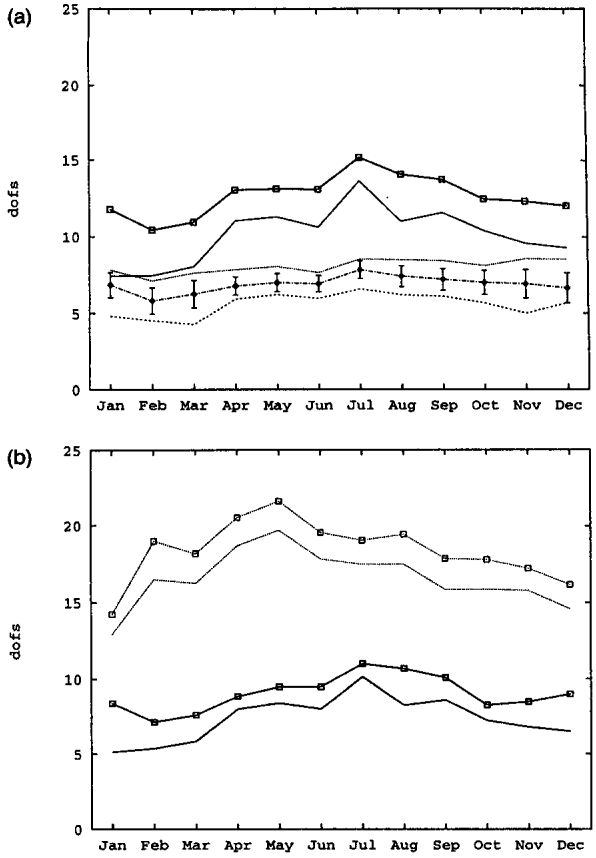

FIG. 3. As in Fig. 1 but for the eastern North Atlantic/European (ENA/EU) sector (30.5°–74.7°N; 61.9°W–33.8°E).

est ones (dof maximum, dof ~ 19–21) in May. Without overstressing the relevance, the occurrence of calendar singularities in the May weather (Bissoli and Schönwiese 1987) could support this result. The dof distributions in the eastern North Atlantic/European sector (Fig. 3) are similar to those of the NH anomalies (Fig. 1), except for a reduction to smaller values.

Dof estimates in the European/Atlantic sector may be compared with the Grosswetter phenomenology: The number of 29 daily weather patterns is about 50% larger than the spatial dimension deduced from unfiltered data and still larger than the dofs of the bandpass-filtered anomalies with a maximum of about dof ~ 22. That is, the phenomenological classification provides more differentiation in the atmosphere than statistical analyses of observations would permit in the dof sense. For the low-pass anomalies, the observed values, dof ~ 5–10, are in general agreement with the ten major Grosswetter regimes to which the 29 daily weather patterns of the North Atlantic/European catalog are combined (Hess and Brezowski 1977). It is interesting to note that Peczely (see Barry and Perry 1973 for reference) set up 13 circulation types for the Atlantic-European region (with a special emphasis on weather around Hungary). This number happens to best coincide with the dof estimate of the anomalies from the monthly means for the same region with an annually averaged value of 13.

c. *ECHAM2 model simulations and observations: A comparison*

General circulation models (GCMs) and observations are traditionally compared by their *phenomenological* behavior (like the number, path, and life cycle of tropical and midlatitude cyclones) and their *physical* properties (e.g., mean temperature anomalies, eddy transports, and energy conversions in the spectral domain). Here we introduce the statistical dimension or spatial degrees of freedom as a scalar measure to make a first step toward a *mathematical* approach of diagnosing model and observational data supplementing phenomenological and physical diagnostics. To date, GCMs have not been tested in this way to any great extent. Therefore, dof analysis is applied, as for the observational data, to the 1000-mb height fields of the Northern Hemisphere and the Atlantic/European sector model data (Figs. 4a–d).

- The ECHAM2 unfiltered anomaly statistics reveal NH-dof estimates that are systematically larger (by

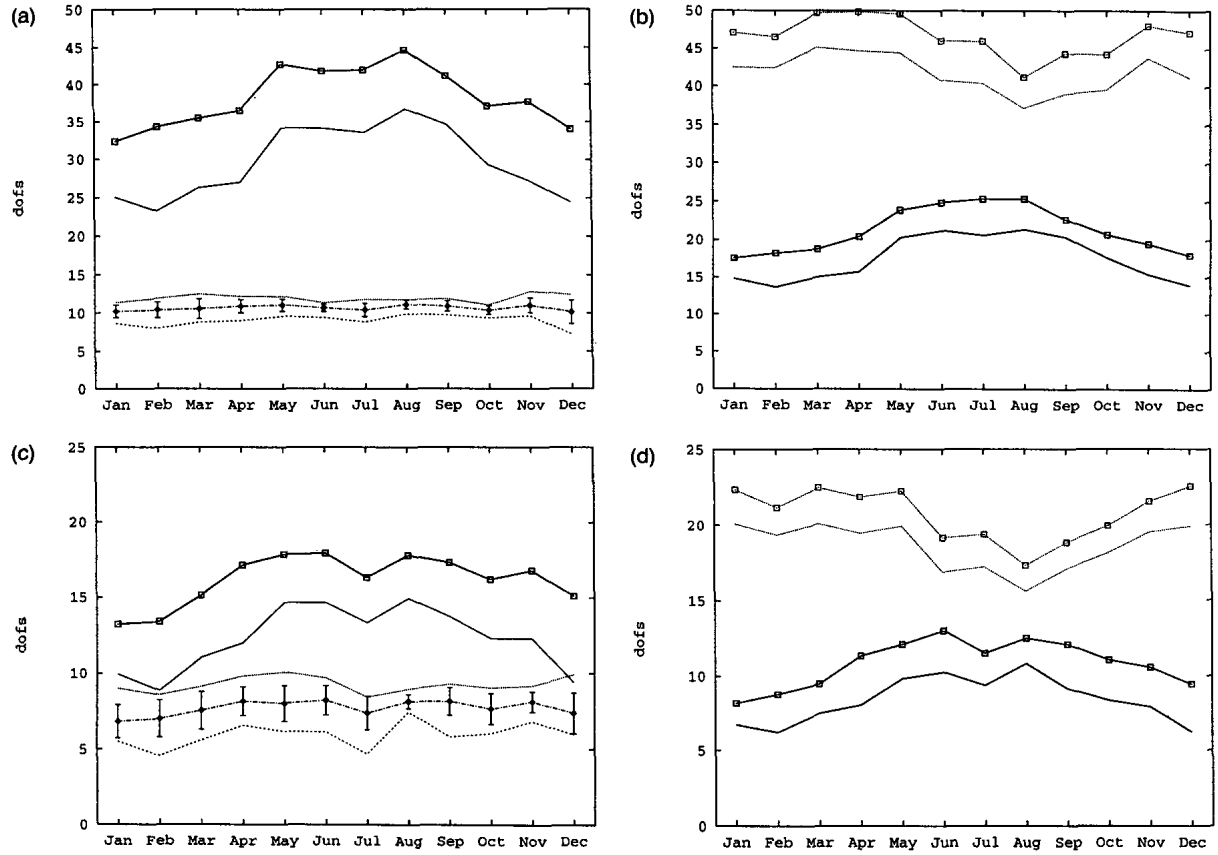

FIG. 4. (a) and (b) As in Fig. 1 but for the ECHAM2 control run. (c) and (d) as in Fig. 3 but for the ECHAM2 control run.

about dof ~ 5) than the observed ones (Fig. 1a). The summer peak has shifted from July to August. As the low-frequency sets of observations and model simulations are qualitatively similar, the difference can be traced to the bandpass filtered processes.

- The bandpass-filtered dataset shows a pronounced simulation-observations difference: The NH-dof estimates of the monthly *and* climate mean anomalies of the control run vary between about dof ~ 47 and ~42; that is, the ECHAM2 simulations show more active modes than the bandpass filtered observations (Figs. 4b and 1b). Moreover, the annual cycle is reversed: the minimum in August (dof ~ 41 and ~ 37) contrasts with the maxima from March to May (dof ~ 50 and ~45). This result may also be related to numerical weather prediction (NWP) performance that appears, on average, to be better in winter than in summer (see Tracton 1993).
- The summer–winter dof-difference between low- and bandpass-filtered eddies is particularly pronounced (Fig. 4b): a large (small) number of independent modes for the low-pass (bandpass) filtered anomalies in summer contrasts the situation in winter. In a qualitative sense one obtains a balance between quasi-stationary (low frequency) and transient (bandpass frequencies) modes contributing in a combined (additive) fashion to the total variability.

Van den Dool and Chervin (1986) compared dimension estimates based on observed data and data from the NCAR climate model. It is interesting that their results for the 500/950 mb thickness and the surface pressure (see their Table 4) are similar to the results presented here in a sense that the model exhibits more degrees of freedom than the observations.

The following results may be relevant for the downscaling problem associated with regional climate response studies: (i) The Atlantic/European sector shows qualitatively similar dof differences between control run and observations but, of course, with smaller values (Figs. 4c, d and Figs. 3c, d). (ii) The simulation–observation difference in dof estimates is most pronounced in lower levels, which determine the climate near the surface (not shown).

An explanation for these simulation–observation differences may be given in qualitative terms. First, one would expect the model to have fewer degrees of freedom (or active modes), because it has a large but still limited number of variables and, therefore, reduced opportunities to interact with other components such as subscale processes. However, this deficiency leads to the opposite effect: The model does not generate a sufficiently small number of dominating and active modes in the bandpass-filtered variability (e.g., weather regimes or blocking). On the contrary, the model tends

to activate a larger number of its own intrinsic modes to cope with the dynamically required constraints due to the limited number of nonlinear interactions that, otherwise, could create a few structurally stable and active flow regimes. That is, the model with limited resolution does not produce as *few* (and possibly realistic) modes as observed in the real atmosphere.

4. Discussion

Measures of nonlinear systems analysis are introduced as a third level of (model and observational) data analysis methods to complement the two traditional diagnostics based on the conventional phenomenological and physical approaches. In this sense the simplified method of estimating the multimodal structure (dimension, dofs, or spatial degrees of freedom) has been introduced as a scalar measure. The analysis is applied to unfiltered, band- and low-pass filtered observational and model data in different spatial domains. Although GCMs have not been tested in this way to any great extent, it is essential to model correctly the nonlinear structure of the atmosphere. Dof estimates may lead to some useful information: (a) The influence of interannual variability can be inferred by the dof difference between the anomalies from monthly means and climate means. (b) The dof estimates of various spatial domains can be compared with numbers of empirically classified weather types. (c) The dof estimates of various timescales yield further information about the scale-dependent number of active modes. (d) As the dof estimates provide the numbers of dynamically active modes in different scales and regions, they can suitably be applied to the simulation–observation comparison. Note that confidence limits and the related sample size need to be considered; 10 years daily data is a relatively small sample for monthly dof estimates. (f) The dof estimate (2.5) may also help as a simple rule of thumb for the number of EOFs that could be used to sufficiently describe the variability of a system [different from the rule used, e.g., by North et al. (1982), and Hsiung and Newell (1983)]. This may be particularly useful in application to extended EOFs in space–time delay coordinates.

Acknowledgments. Thanks are due to Dr. Z. Toth for sending preprints of his papers, Ms. Judith Perlwitz and Dr. H. von Storch for stimulating discussions. Dr. Toth's and another reviewer's constructive comments are appreciated, and Dr. D. Gutzler's helpful editorial assistance. Part of the research is related to a BMFT grant on climate variability.

APPENDIX

Statistical Dimension (Degrees of Freedom) of Normally Distributed Variables ($N > 2$)

Let X_i (or X) be Gaussian distributed variables. The degrees of freedom (or number of independent variables) is defined such that the variance of the sum of the squared variables X_i standardized by their number N, equals the variance of a chi-squared variable standardized by its degrees of freedom:

$$\mathrm{var}\Big(\sum_{i=1}^{N} X_i^2/N\Big) = \mathrm{var}\Big(\sum_{i=1}^{N} X_i^2\Big)/N^2 = \mathrm{var}(\chi^2_{\mathrm{dof}}/\mathrm{dof})$$

$$= \mathrm{var}(\chi^2_{\mathrm{dof}})/\mathrm{dof}^2 = 2/\mathrm{dof} \qquad \text{(A1)}$$

or

$$\mathrm{dof} = 2N^2/\mathrm{var}\Big(\sum_{i=1}^{N} X_i^2\Big), \qquad \text{(A2)}$$

because the mean (variance) of a chi-squared variable with dof degrees of freedom is 1 dof (2 dof). We can write the covariance matrix C of the dependent variables X_i as $C = S\Lambda S^{-1} = \langle XX^T \rangle$ with the diagonal eigenvalue matrix Λ and the eigenvector matrix S (which is orthogonal, $S^{-1} = S^T$). The new independent normalized variables $\xi = \Lambda^{-1/2}S^{-1}X$, whose covariance matrix C' equals the identity matrix I, can be derived:

$$C' = \langle \xi\xi^T \rangle = \Lambda^{-1/2}S^{-1}\langle XX^T \rangle S\Lambda^{-1/2}$$

$$= \Lambda^{-1/2}S^{-1}S\Lambda S^{-1}S\Lambda^{-1/2} = I. \qquad \text{(A3)}$$

The dependent variable X can be expressed by the independent variables $X = S\Lambda^{1/2}\xi$. We may now write the sum of the squares

$$\sum_{i=1}^{N} X_i^2 = X^TX = (S\Lambda^{1/2}\xi)^T(S\Lambda^{1/2}\xi)$$

$$= \xi^T\Lambda^{1/2}S^{-1}S\Lambda^{1/2}\xi = \xi^T\Lambda\xi = \sum_{i=1}^{N} \lambda_i\xi_i^2$$

$$= \lambda_1\xi_1^2 + \lambda_2\xi_2^2 + \cdots \lambda_N\xi_N^2,$$

because $\xi^T\Lambda^{1/2}S^TS\Lambda^{1/2}\xi = \xi^T\Lambda^{1/2}S^{-1}S\Lambda^{1/2}\xi$. Taking variances on both sides yields $\mathrm{var}(\sum_{i=1}^{N} X_i^2) = \mathrm{var}(\lambda_1\xi_1^2 + \lambda_2\xi_2^2 + \cdots)$. Since the ξ_i are independent, the variance of the sum on the right-hand side equals the sum of the variances, $\mathrm{var}(\sum_{i=1}^{N} X_i^2) = \lambda_1^2\,\mathrm{var}(\xi_1^2) + \lambda_2^2\,\mathrm{var}(\xi_2^2) + \cdots$. Furthermore, all ξ_i^2 are chi-squared (χ_1^2) distributed with one degree of freedom, so that their variance is 2, then

$$\mathrm{var}\Big(\sum_{i=1}^{N} X_i^2\Big) = 2\sum_{i=1}^{N} \lambda_i^2. \qquad \text{(A4)}$$

Substituting (A4) into (A2) finally yields

$$\mathrm{dof} = N^2/\sum_{i=1}^{N} \lambda_i^2. \qquad \text{(A5)}$$

Now, taking the $N = 2$ variables X_1 and X_2, the covariance matrix $C = \langle (X_1, X_2)(X_1, X_2)^T \rangle$ has the eigenvalues $\lambda_1 = 1 + c$ and $\lambda_2 = 1 - c$, so that $\sum_{i=1}^{2} \lambda_i^2 = 2(1 + c^2)$ or (2.4) is verified. Finally, it

should be noted that the derivation of (A5) is only valid for multinormally distributed variables.

REFERENCES

Barry, R. G., and A. H. Perry, 1973: *Synoptic Climatology, Methods and Applications.* Methuen & Co. Ltd., 555 pp.

Bissolli, P., and C. D. Schönwiese, 1987: Singularitäten in der Bundesrepublik Deutschland 1946–1986. Vorläufige Ergebnisse einer statistischen Analyse anhand ausgewählter Stationen. *Meteor. Rundsch.*, **40,** 147–155.

Blackmon, M. L., 1976: A climatological spectral study of the 500 mb height of the Northern Hemisphere. *J. Atmos. Sci.*, **33,** 1607–1623.

——, and N.-C. Lau, 1980: Regional characteristics of the Northern Hemisphere winter time circulation: A comparison of a GFDL general circulation model with observations. *J. Atmos. Sci.*, **37,** 497–514.

Cheng, X., and J. M. Wallace, 1993: Cluster analysis of the Northern Hemisphere wintertime 500 hPa height field: Spatial patterns. *J. Atmos. Sci.*, **50,** 2647–2696.

Dzerdzeevskii, B. L., 1975: *The Observed Circulation of the Atmosphere and Climate* (in Russian). 285 pp.

Gerstengarbe, F.-W., and P. C. Werner, 1993: Katalog der Großwetterlagen Europas nach Hess und Brezowski 1881–1992. *Ber. Dtsch. Wetterdienstes,* **113,** 249 pp.

Hess, P., and H. Brezowski, 1977: Katalog der Grosswetterlagen. *Ber. Dtsch. Wetterdienstes,* **113,** 39 pp.

Horel, J. D., 1985: Persistence of the 500 mb height field during Northern Hemisphere winter. *Mon. Wea. Rev.*, **113,** 2030–2042.

Hsiung, J., and R. E. Newell, 1983: The principal nonseasonal modes of variation of global sea surface temperature. *J. Phys. Oceanogr.*, **13,** 1957–1967.

Kimoto, M., and M. Ghil, 1993a: Multiple flow regimes in the Northern Hemisphere winter. Part I: Methodology and hemispheric regimes, *J. Atmos. Sci.*, **50,** 2625–2643.

——, and ——, 1993b: Multiple flow regimes in the Northern Hemisphere winter. Part II: Sectorial regimes and preferred transitions. *J. Atmos. Sci.*, **50,** 2645–2673.

Lamb, H. H., 1972: British Isles weather types and a register of the daily sequence of circulation patterns, 1861–1971. *Geophys. Mem.*, **116,** 85 pp.

Livezey, R. E., and W. Y. Chen, 1983: Statistical field significance and its determination by Monte Carlo techniques. *Mon. Wea. Rev.*, **111,** 49–59.

Lorenz, E. N., 1969: Atmospheric predictability as revealed by naturally occurring analogues. *J. Atmos. Sci.*, **26,** 636–646.

Molteni, F., S. Tibaldi, and T. N. Palmer, 1990: Regimes in the wintertime circulation over northern extratropics. I: Observational evidence. *Quart. J. Roy. Meteor. Soc.*, **116,** 31–67.

North, G. R., T. L. Bell, R. F. Cahalan, and F. J. Moeng, 1982: Sampling errors in the estimation of empirical orthogonal functions. *Mon. Wea. Rev.*, **110,** 699–706.

Roeckner, E., K. Arpe, L. Bengtson, S. Brinkop, L. Dümenil, W. Esch, E. Kirk, F. Lunkeit, M. Ponater, B. Rockel, R. Sausen, U. Schlese, S. Schubert, and M. Windelband, 1992: Simulation of the present-day climate with the ECHAM model: Impact of model physics and resolution. Max-Planck-Institut für Meteorologie, Report No. 93, 172 pp.

Toth, Z., 1994: Dimension estimates of the Northern Hemisphere circulation phase space. *Tellus,* **46A.**

Tracton, M. S., 1993: On the skill and utility of NMC's medium range central guidance. *Wea. Forecasting,* **8,** 147–153.

Van den Dool, H. M., and R. M. Chervin, 1986: A comparison of month-to-month persistence of anomalies in a general circulation model and in the earth's atmosphere. *J. Atmos. Sci.*, **43,** 1454–1466.

Vautard, R., 1990: Multiple weather regimes over the North Atlantic: Analysis of precursors and successors. *Mon. Wea. Rev.*, **118,** 2056–2081.

Wallace, J. M., and Y. Zhang, 1993: Structure and seasonality of interannual and interdecadal variability of the geopotential height and temperature fields in the Northern Hemisphere troposphere. *J. Climate,* **6,** 2063–2082.